ARTICLE IN PRESS

Available online at www.sciencedirect.com

ScienceDirect

Acta Materialia xxx (2013) xxx–xxx

Acta MATERIALIA

www.elsevier.com/locate/actamat

Deformation response of ferrite and martensite in a dual-phase steel

H. Ghassemi-Armaki [a], R. Maaß [b], S.P. Bhat [c], S. Sriram [c], J.R. Greer [b,d], K.S. Kumar [a,*]

[a] *School of Engineering, Brown University, Providence, RI 02912, USA*
[b] *Division of Engineering & Applied Sciences, California Institute of Technology, Pasadena, CA 91125, USA*
[c] *ArcelorMittal, Global R & D, East Chicago, IN 46312, USA*
[d] *The Kavli Nanoscience Institute at Caltech, Pasadena, CA 91125, USA*

Received 2 June 2013; received in revised form 30 September 2013; accepted 2 October 2013

Abstract

Deformation response of ferrite and martensite in a commercially produced dual-phase sheet steel with a nominal composition of 0.15% C–1.45% Mn–0.30% Si (wt.%) was characterized by nanoindentation and uniaxial compression of focused ion beam-milled cylindrical micropillars (1–2 μm diameter). These experiments were conducted on as-received and pre-strained specimens. The average nanoindentation hardness of ferrite was found to increase from ~2 GPa in the as-received condition to ~3.5 GPa in the specimen that had been pre-strained to 7% plastic tensile strain. Hardness of ferrite in the as-received condition was inhomogeneous: ferrite adjacent to ferrite/martensite interface was ~20% harder than that in the interior, a feature also captured by micropillar compression experiments. Hardness variation in ferrite was reversed in samples pre-strained to 7% strain. Martensite in the as-received condition and after 5% pre-strain exhibited large scatter in nanoindentation hardness; however, micropillar compression results on the as-received and previously deformed steel specimens demonstrated that the martensite phase in this steel was amenable to plastic deformation and rapid work hardening in the early stages of deformation. The observed microscopic deformation characteristics of the constituent phases are used to explain the macroscopic tensile deformation response of the dual-phase steel.

Keywords: Dual-phase steel; Mechanical behavior; Nanoindentation; Micropillar compression; Electron microscopy

1. Introduction

Dual-phase sheet steels find widespread use in the automotive sector for structural applications. Their high strength-to-weight ratio, low yield-to-ultimate strength ratio combined with a high initial work hardening rate and good formability make them particularly suited for these applications. These steels in the fully heat-treated condition are composed of ferrite and martensite, but sometimes can include ferrite and cementite with a bainitic morphology as well. In this paper, we limit the discussion to dual-phase steels composed of martensite and ferrite as they constitute the most relevant microstructure. The fraction of the hard martensite phase embedded in the softer ferrite phase ranges anywhere from 10 to >50 vol.% [1–5]. The specific steel grade investigated falls in the general category of 980DP steels, which are often used in automotive bumper applications.

The uniaxial tensile deformation response of these steels has been extensively studied over the past two or three decades; a general picture that emerges from these studies is that there exists an initial deviation from Hooke's law, signifying that the elastic limit is followed by continuous yielding and a high strain hardening rate, before a second change to a shallower work hardening rate occurs, which eventually leads to an ultimate tensile strength, neck formation and final fracture. The exact stress and strain levels at which these events occur are dependent on the composition of the steel, the volume fraction of the coexisting phases, their relative sizes, their distribution and their morphology [6–12]. Although the initial yielding is associated

* Corresponding author.
E-mail address: Sharvan_Kumar@brown.edu (K.S. Kumar).

1359-6454/$36.00
http://dx.doi.org/10.1016/j.actamat.2013.10.001

Please cite this article in press as: Ghassemi-Armaki H et al. Deformation response of ferrite and martensite in a dual-phase steel. Acta Mater (2013), http://dx.doi.org/10.1016/j.actamat.2013.10.001

with the plastic deformation of ferrite, the stress and strain for the initial onset of plastic flow in martensite and the subsequent partitioning of plastic strain between the two phases as global deformation ensues have been points of discussion, debate and ongoing research [13–19].

The austenite–martensite transformation in these dual-phase steels is accompanied by a 2–4 vol.% change that is instrumental in generating residual stresses in the ferrite as well as producing geometrically necessary dislocations in the ferrite close to the ferrite/martensite interface [5,20,21]. Such geometrically necessary dislocations (GNDs) have been observed by transmission electron microscopy (TEM) and quantified by high-resolution electron backscattered diffraction (EBSD). The residual stresses are thought to be responsible for enhancing plastic flow in ferrite and for lowering the elastic limit, while the unpinned GNDs are thought to contribute to the continuous initial yielding as well as the observed initial strain hardening rate [5,22].

Recent advances in mechanical testing techniques at the microscale, including nanoindentation and micro- and nanopillar compression testing, have made it possible to ascertain properties of micron- and sub-micron-size single crystal regions/specimens of many metals and alloys. Numerous research articles and exhaustive reviews of advances in the field that also describe benefits and shortcomings of the testing techniques and their future potential are available, a few of which are cited here [23–34]. These techniques can also be applied to characterize the mechanical response of micron-scale individual phases in multiphase alloys.

Nanoindentation enables probing the mechanical response of individual phases in the size range between 1 and 10 μm in a multiphase alloy. The challenge lies in converting the obtained load–displacement data into a stress–strain curve (particularly in the plastic regime) that could form the input for computations or for making scientific connection with the global response of the alloy that is usually in the form of stress–strain curves. Several attempts have been made to extract portions of the plastic tensile stress–strain curve from nanoindentation data [24,26–28,35,36], but debate continues about the validity of such approaches. Choi et al. [26] attempted to predict the macroscopic plastic deformation response of a dual-phase steel from nanoindentation response of the constituent phases using two spherical indenter tips, while Delincé and coworkers [25] used different nanoindentation depths to isolate strengthening mechanisms in a dual-phase steel composed of ferrite and martensite. Recently, Kadkhodapour et al. [5] have used nanoindentation to probe the presence of GNDs in ferrite in the vicinity of the ferrite/martensite interface in a dual-phase steel. Nanoindentation has also been used to isolate the role of microstructure on lath martensite strength, and it was concluded from such studies that block boundaries are important in strengthening Fe–C martensite [37–39].

Uniaxial compression of micropillars machined using a focused ion beam (FIB) is another technique that can be used to assess mechanical properties in small volumes. Numerous studies have been performed on a wide range of materials using this technique; many metallic and ceramic materials, and especially those in which plastic deformation occurs by crystallographic slip, have been reported to exhibit a strong size effect in strength for sample sizes in the range between several microns and tens of nanometers [29–33,40–46]. In single crystalline face-centered cubic metals, this size effect has been attributed to dislocation source truncation, exhaustion hardening, source-driven plasticity and dislocation starvation [29–32]. Body-centered cubic (bcc) metals also exhibit size effects, which are unique to each individual material because of the more complex dislocation mobility in these metals [42–46].

The micropillar approach has been adopted for examining the mechanical response of a low-carbon martensite and has demonstrated that, while a single martensite block may exhibit elastic–perfectly plastic behavior, the presence of boundaries in the form of blocks and packets leads to significant hardening [47]. Stewart et al. [48] used similar micropillar compression tests to document the deformation behavior of constituent phases in a dual-phase stainless steel produced by powder metallurgy, and the results were utilized in a rule-of-mixture-type model after correcting for porosity to predict the ultimate tensile strength of the steel. The influence of crystallographic orientation on yield stress and subsequent hardening was not isolated, nor was post-deformation microstructure analyzed to ensure that the micropillars were single phase throughout their height.

In this work, we conducted nanoindentation and micropillar compression experiments to obtain the micromechanical response of the individual ferrite and martensite phases in a 0.15 wt.% C dual-phase sheet steel in the as-received condition. Macroscopic uniaxial tensile tests were performed using dog-bone geometry specimens excised from the sheet to obtain the overall stress–strain response. Tensile tests were performed to various strains along the stress–strain curve and unloaded. Micropillars were excised from the ferrite and martensite phases in these interrupted test specimens to understand how the global deformation influenced the properties of the individual phases. The microstructures of deformed micropillars were analyzed via TEM. The mechanical data and microstructural evolution obtained served to interpret the deformation response of the dual-phase steel. Plastic deformation and rapid hardening of martensite are recognized and their contribution to the deformation response of the dual-phase steel is considered.

2. Experimental procedure

The material examined in this study is a dual-phase sheet steel with a thickness of 2 mm and a nominal

Please cite this article in press as: Ghassemi-Armaki H et al. Deformation response of ferrite and martensite in a dual-phase steel. Acta Mater (2013), http://dx.doi.org/10.1016/j.actamat.2013.10.001

chemical composition of 0.15% C–1.45% Mn–0.30% Si (wt.%), processed on a water-quenched continuous anneal line. The manufacturing steps include an inter-critical anneal followed by water quenching at an approximate cooling rate of 1000 °C s^{-1} and a low-temperature overaging at about 200 °C. In the commercially processed condition, the microstructure is composed roughly of 0.6 and 0.4 volume fractions of ferrite and martensite, respectively. Uniaxial tensile samples with a 25.4 mm gauge length and flat dog-bone geometry were cut initially parallel, perpendicular and at 45° to the rolling direction to assess possible variations in the tensile response as a consequence of any in-plane anisotropy that might have been present, but none was observed. Consequently, all tensile specimens were subsequently cut parallel to the rolling direction. Interrupted tensile tests were also performed to obtain specimens with different levels of plastic strain (0.5%, 5% and 7%) for further characterization of the deformed microstructure and its evolution with strain, as well as to enable assessment of the micromechanical properties of the individual phases as a function of the global plastic strain in the dual-phase steel.

Sections cut from the deformed samples were mechanically ground and polished and finally electropolished in an aqueous electrolyte consisting of perchloric acid:ethanol in a 1:9 ratio (20 V, −40 °C). Nanoindentation tests were conducted using a Hysitron Triboscope nanoindenter equipped with a Berkovich tip. The maximum indentation force was selected such that the size of the indentation was not large enough to exceed the average grain size of the individual phases (ferrite and martensite) but not so small so that surface roughness dominates the outcome. The appropriate maximum force was determined to be in the vicinity of 2500 μN, and this was the force that was used for all nanoindentation tests reported in this paper. An array of 400 nanoindentations were made on each specimen, with an indentation spacing interval of ∼6 μm; each specimen was then examined in a dual-beam FEI scanning electron microscope–FIB to determine the location of each of the indentations. Indentations which traversed ferrite/ferrite or martensite/ferrite interfaces were eliminated and the rest were binned into three groups: the first group included indentations that were inside ferrite and far from any interface, the second group included those that were in the ferrite but close to the martensite/ferrite interface with a maximum distance of 2–3 μm from the interface, and the third group of indentations consisted of those that were located inside martensite.

Uniaxial compression experiments were performed on the micropillars fabricated within the individual ferrite and martensite phases in the as-received sheet as well as from the post-deformed tensile specimens that were strained to various levels. These tests were performed using the Hysitron Triboscope nanoindenter with a 10 μm diameter diamond flat punch. The diameters of the micropillars were between 1 μm and 2 μm, with an aspect ratio ⩾2. These cylinders were milled using an established top-down methodology [29] in the dual-beam FIB (FEI, Helios Nanolab 600 dual beam FIB) using 30 keV Ga ions with progressively lower currents, starting with 20 nA and ending with ∼9.7 pA. The ferrite micropillars, with diameters of ∼2 μm, were milled in the grains that were larger than 10 μm, while the martensite micropillars, with diameters of ∼1.0–1.5 μm, were milled from the largest martensite islands, the dimensions of which ranged from 6 to 8 μm, to ensure that the milled micropillars were centered in the martensite grains and away from the martensite/ferrite interfaces. Such top-down methodology has been shown to create a slight vertical taper along the height of the cylinder [29]; the diameters at the top surface and at a location a third of the way up from the bottom of each micropillar were measured and averaged to calculate the nominal stress. In instances where the top surface of the micropillar was rough, for example, as a result of prior light etching to distinguish the two phases, a thin layer was milled off from the top surface by FIB-assisted etching. The micropillar surface normal was determined by EBSD, which revealed that the orientation within a single ferrite micropillar varied by no more than 2° whereas in martensite the orientation varied with location on the top surface of the pillar, the extent varying from pillar to pillar. The latter observation is consistent with the hierarchically scaled microstructure within martensite consisting of laths, blocks and packets.

All the micropillar compression tests were conducted at a nominal constant strain rate of 10^{-3} s^{-1}. The goal of this set of experiments was to determine the stress for onset of plastic flow and an appreciation for early stage hardening, and so the reported stress–strain curves were truncated at ∼5% strain even though the actual tests were carried out to higher strains. The microstructure of the deformed micropillars was examined in the transmission electron microscope by preparing samples via the established “lift-out” method [49]. The aim of such TEM analysis was to verify that the compressed micropillars contained a single phase. Such specimens were then Pt-bonded to a Cu grid and examined in a CM20 Philips transmission electron microscope operating at 200 kV.

3. Results

3.1. As-received microstructure and tensile σ–ε response

The scanning electron microscopy (SEM) image of a polished and etched section of the dual-phase steel in the as-received condition in Fig. 1a illustrates a microstructure consisting of a mixture of ferrite and martensite. The ferrite regions, which range in size from about 4–15 μm, are typically surrounded by a somewhat discontinuous necklace of martensite regions which are typically less than 10 μm. TEM indicates a high dislocation density in ferrite and the presence of fine Fe-carbide particles that are effective in pinning dislocations (Fig. 1b and c); the martensitic structure consists of blocks, packets and laths that are

Please cite this article in press as: Ghassemi-Armaki H et al. Deformation response of ferrite and martensite in a dual-phase steel. Acta Mater (2013), http://dx.doi.org/10.1016/j.actamat.2013.10.001

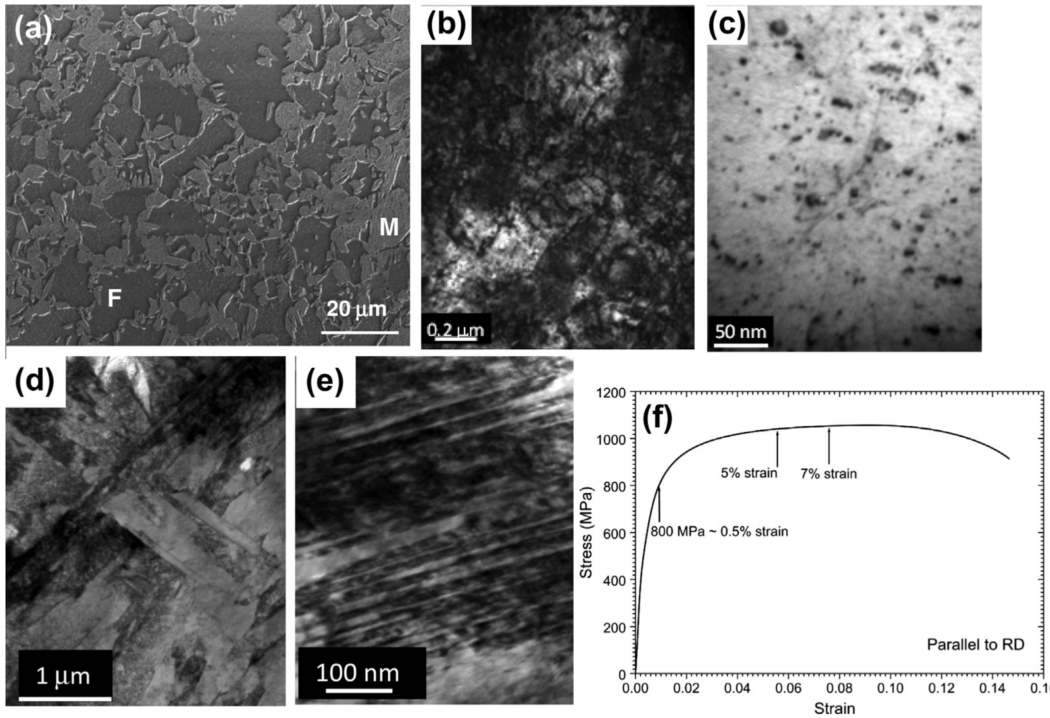

Fig. 1. (a) A representative SEM image of the as-rolled dual-phase steel microstructure composed of ferrite and martensite. TEM bright-field images illustrating a high dislocation density and fine carbide particles in ferrite (b and c), martensite morphology showing packets, blocks and laths (d and e), and (f) uniaxial tensile response (engineering stress-engineering strain) of this steel. The arrows in (f) indicate the locations where duplicate tests were interrupted to obtain samples for nanohardness measurements and micropillar compression tests. RD in (f) denotes rolling direction.

typical of low-carbon lath martensite, with the lath size ranging from 30 to 100 nm (Fig. 1d and e). The uniaxial macroscopic tensile stress–strain response of this dual-phase sheet steel (Fig. 1f) shows the onset of yielding at around 350 MPa; beyond this stress level, a deviation from linearity is noted, with a steep hardening response until about 750 MPa. Beyond 750 MPa, the slope decreases continuously until the ultimate tensile strength of 1050 MPa is reached at 9.5% strain; final fracture occurs at a strain of ~15%. The arrows in Fig. 1f correspond to the stresses and strains at which duplicate tests were interrupted to obtain specimens for further characterization with prescribed levels of tensile deformation.

3.2. Micromechanical response of the individual phases: as-received condition

The mechanical response of the individual phases, ferrite and martensite, in the as-received condition was probed using nanoindentation and micropillar compression tests and the results are presented in this section; further, the micropillar response obtained for the ferrite phase is compared to the response for pure bcc iron.

3.2.1. Ferrite

An SEM image of ferrite exhibiting five nanoindentations is shown in Fig. 2a, the indentations being labeled 1–5. Indentation 1 is <1 μm from the ferrite/martensite interface, whereas indentations 2–5 are further into the interior of ferrite and away from the interfaces. The resulting force–displacement profiles for the five indentations are shown in Fig. 2b. Indentation 1, close to the ferrite/martensite interface, displays a hardness of 5.8 GPa and an indentation depth of ~80 nm; indentations 2–5 are 120–130 nm deep and have lower hardness values of 3.5 ± 0.1 GPa (mean ± standard deviation). The distribution of nanohardness is presented as a cumulative undersize vs. hardness plot for interior ferrite and for ferrite close to the ferrite/martensite interface in Fig. 2c. The nanohardness of the interior ferrite ranged from 1.5 to 5.5 GPa at the extremes, with a significant fraction of samples having a hardness between 2.2 and 3.8 GPa; the comparable range for ferrite close to the ferrite/martensite interface was 3–4.8 GPa. The spread in data is in part dependent on the orientation of individual grains from which the data were collected, as well as on the variation in substructure from grain to grain. A comparison of the hardness for 50% undersize indicates the interior ferrite to be $\sim 3.3 \pm 0.89$ GPa and that for the ferrite near the ferrite/martensite interface to be $\sim 3.9 \pm 0.95$ GPa. These results are in accordance with previous observations and the proposal that the formation of GNDs in ferrite close to the ferrite/martensite interface during transformation of austenite to martensite can result in local hardening of ferrite [5].

We next characterized the ferrite using micropillar compression tests. We first demonstrated reproducibility by testing two micropillars that were milled within a single

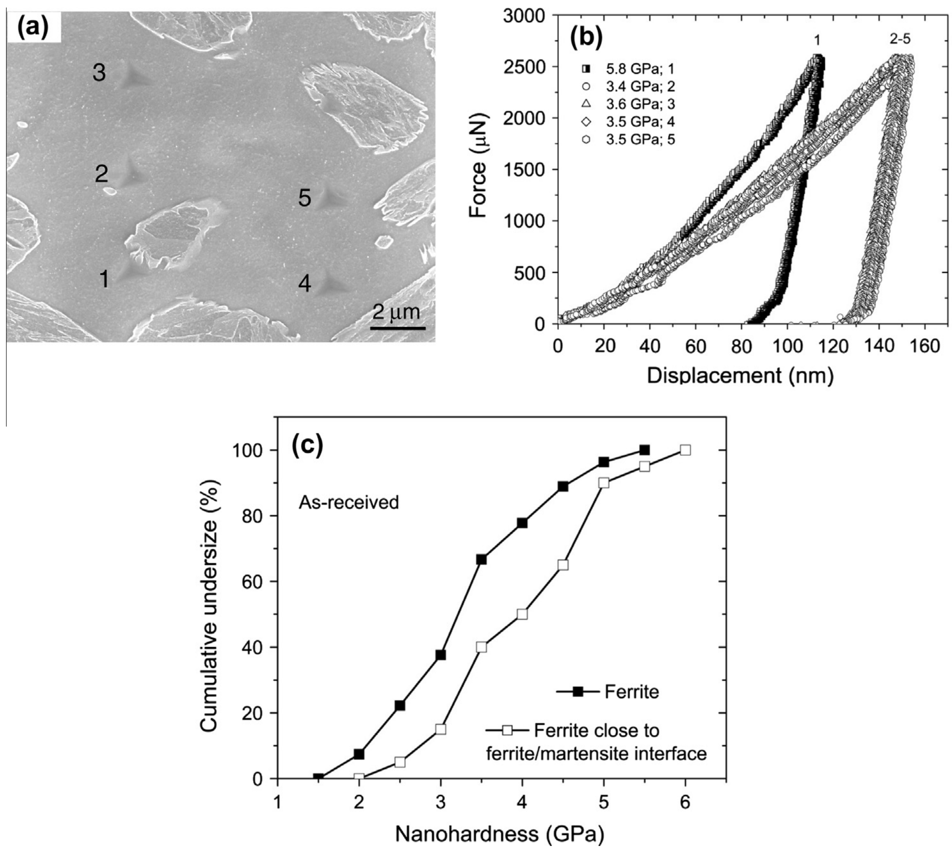

Fig. 2. (a) SEM image showing five nanoindentation impressions (labeled 1–5) in ferrite; 1 is close to the ferrite/martensite interface, whereas 2–5 are in the interior of ferrite. (b) The corresponding force–displacement curves for the five nanoindentations. (c) Nanohardness distribution curves (cumulative undersize plots) for ferrite in the interior and for ferrite close to the ferrite/martensite interface in the as-rolled sample.

ferrite grain, both far from the ferrite/martensite interface (micropillars A and B in Fig. 3a). The EBSD image for the grain is shown in Fig. 3b and the uniaxial compression stress–strain data obtained from these two micropillars are shown in Fig. 3c, along with an inverse pole figure (IPF). The ferrite grain normal was close to [1 1 1], with a loading axis corresponding specifically to [2 2 3]. The compressive stress–strain curves for the two micropillars were similar, which confirmed self-consistency. (The appearance of load drops in these stress–strain curves is a manifestation of small-scale plasticity. Sudden slip events lead to forward surges of the compression tip in displacement-controlled tests.) SEM images of the two deformed micropillars revealed a similar deformation pattern of single slip where the top shears off, as shown in Fig. 3d and e.

After this validation procedure, additional micropillars were milled from several ferrite grains whose orientations were determined by EBSD. The uniaxial compression stress–strain curves for seven such micropillars obtained from different grains are shown in Fig. 4a. Crystal orientations of each sample, which correspond to the loading axis in the micro-compression experiments, are shown within an inverse pole figure in Fig. 4b and are listed in Table 1.

Most of the pillars (F1, F4, F5, F6 and F7) had their loading axis close to [1 1 1]; one pillar (F2) was located in the middle of the IPF and another (F3) was located in the vicinity of [0 0 1]. The stress of 220 GPa at the onset of yielding was lowest for the F2 micropillar with a loading axis of [3 1 5], and lower than the overall range of 350–450 MPa for the rest of the pillars (Fig. 4a; Table 1). The onset of yielding in this paper is determined by plotting the incremental slope of the engineering stress–strain curve ($d\sigma/d\varepsilon$) as a function of engineering stress (σ) and identifying the stress at which the slope of this curve changes discontinuously (an example for martensite micropillars is presented later in Fig. 14). The resolved shear yield stress was calculated for each of the seven ferrite micropillars, assuming that slip occurred in each of them on the system with the highest Schmid factor, and the data are reported in Table 1. All 48 bcc slip systems were considered ($\{1 1 0\}\langle -1 1 1\rangle$; $\{2 1 1\}\langle -1 1 1\rangle$ and $\{3 2 1\}\langle -1 1 1\rangle$), and it is noted that the average shear yield value is around 145 MPa (see Table 1). The possibility of breakdown in Schmid's law, which has been reported for several pure bcc metals [50], is not considered here (these micropillars include a high initial dislocation density and contain C and Mn in solid solution, all of which present additional components of internal elastic strains that affect the screw dislocation core configuration in unknown ways; while the influence of interstitials (C, N) on the hardening and softening of Fe has been studied and explained on the basis of screw dislocation motion [51,52], less is known about

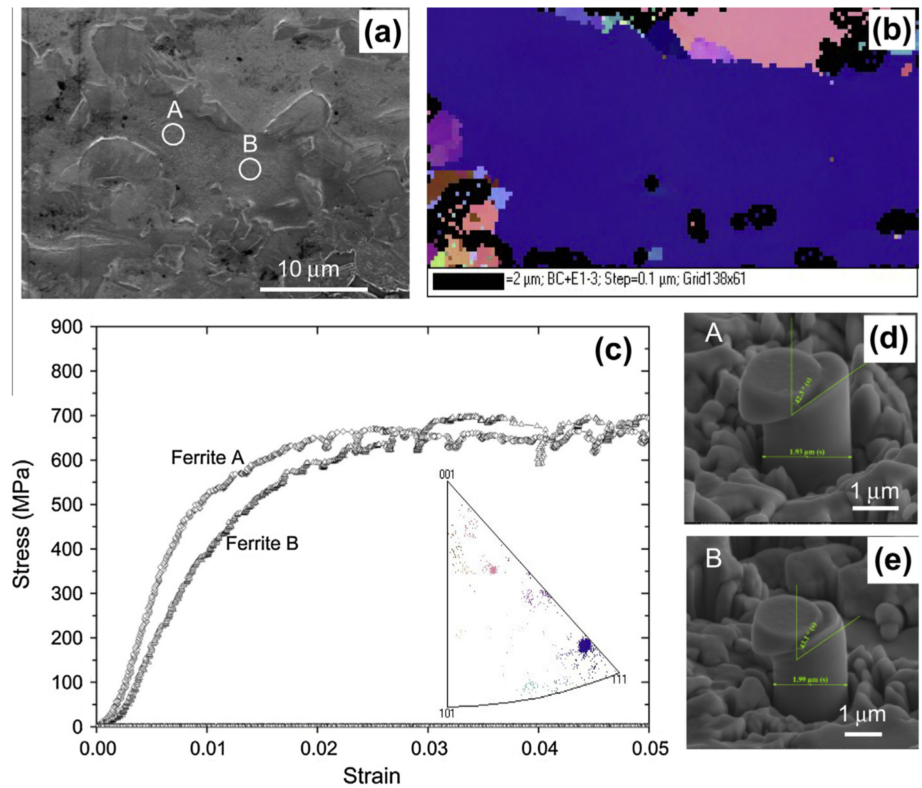

Fig. 3. (a) A large ferrite grain indicating the locations (white circles) where two micropillars, A and B, were FIB-milled; (b) EBSD of the ferrite grain; (c) compression engineering stress–engineering strain curves from the micropillars (inset: IPF isolating the orientation of the ferrite grain from (b)); and (d and e) SEM images of the two micropillars after deformation illustrating reproducible deformation pattern.

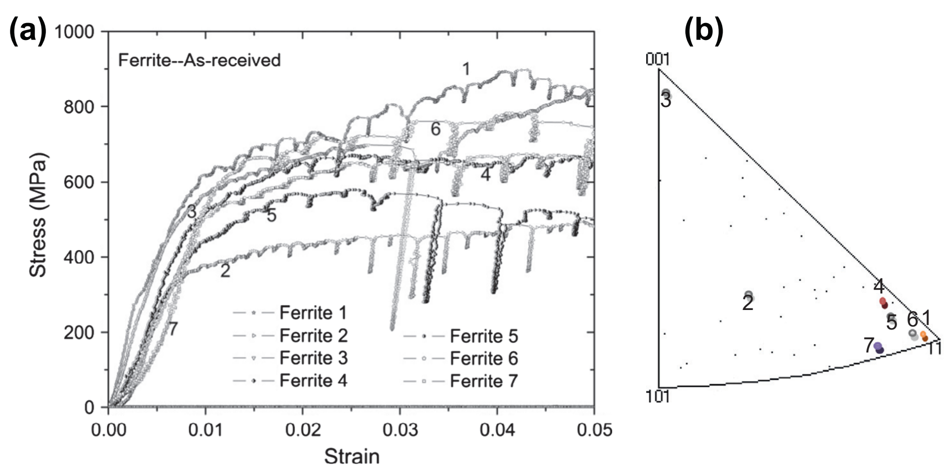

Fig. 4. (a) Compression engineering stress–engineering strain curves for ~2 μm diameter ferrite micropillars (1–7) obtained from different ferrite grains; (b) IPF indicating the crystal orientation of each ferrite grain from which pillars F1–F7 were milled.

how they precisely modify the screw dislocation core structure of Fe). If this average shear yield stress of 145 MPa is multiplied by the Taylor factor of 2.73 (for pencil glide [53]), we obtain a polycrystalline compressive yield strength of ~395 MPa, which is in reasonable agreement with the stress level of ~350 MPa, where the tensile stress–strain curve for the dual-phase steel shows an initial deviation from linearity in Fig. 1f. It is appropriate to point out that steels, even in a well-annealed condition, are known to exhibit "strength differential" effects in tension vs. compression [54,55], so caution should be exercised in interpreting these results.

The compression response of ferrite described above is compared to that of annealed pure Fe in Fig. 5a and b for loading along the [1 1 1] and [0 0 1] directions, respectively. It is evident that the stress values for the onset of yielding and hardening rates of ferrite are higher than those for pure iron. Recognizing that the pure Fe specimens are

Table 1
Loading axis and stress at onset of yield for ferrite micropillars.

Nomenclature	Loading axis orientation	Onset of compressive yield (MPa)	Dominant slip system (s)	Schmid factor	Resolved shear stress for yielding (MPa)
AR[a]-F1	[7 7 8]	∼400	{1 2 1}⟨1 −1 1⟩ {2 1 1}⟨−1 1 1⟩	0.34	∼135
AR-F2	[3 1 5]	∼220	{1 3 2}⟨1 −1 1⟩	0.49	∼110
AR-F3	[0 0 1]	∼400	{−1 1 2}⟨1 −1 1⟩{1 −1 2}⟨−1 1 1⟩	0.47	∼185
AR-F4	[2 2 3]	∼400	{1 2 1}⟨1 −1 1⟩ {2 1 1}⟨−1 1 1⟩	0.36	∼145
AR-F5	[3 3 4]	∼350	{1 2 1}⟨1 −1 1⟩ {2 1 1}⟨−1 1 1⟩ {1 3 2}⟨1 −1 1⟩ {3 1 2}⟨−1 1 1⟩	0.36	∼125
AR-F6	[5 5 6]	∼450	{1 2 1}⟨1 −1 1⟩ {2 1 1}⟨−1 1 1⟩ {1 3 2}⟨1 −1 1⟩ {3 1 2}⟨−1 1 1⟩	0.34	∼155
AR-F7	[5 4 6]	∼450	{0 1 1}⟨1 −1 1⟩	0.37	∼165
0.5% Plastic strain	[4 5 6]	∼400	{2 1 1}⟨−1 1 1⟩	0.41	∼165
7% Plastic strain	[4 4 5]	∼550	{1 2 1}⟨1 −1 1⟩	0.35	∼190

[a] AR denotes as-received condition.

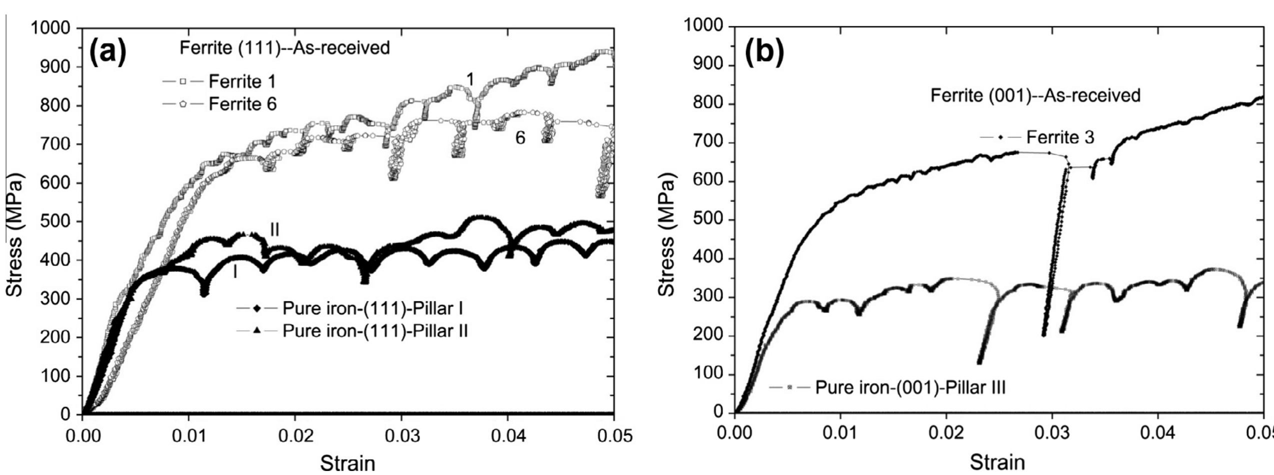

Fig. 5. A comparison of the compression engineering stress–engineering strain curves for annealed pure Fe micropillars with those for ferrite micropillars: (a) (1 1 1) and (b) (0 0 1) loading axes.

in a fully annealed state whereas the ferrite pillars are heavily dislocated, having been milled from a commercial as-produced steel, and contain Mn in solid solution and fine carbide particles resulting from the heat treatment, it is not surprising that both the yield strength and the early stage work hardening response of ferrite are higher than that for the pure Fe for a given loading axis.

The nanoindentation results presented in Fig. 2c and d show that the hardness of ferrite close to the ferrite/martensite interface is higher than that in the center of the ferrite grains. Such measurements suffer from the proximity of the indentation location to the interface, with the consequence that the hard martensite phase could impose a constraint on plastic deformation of the softer ferrite phase, particularly below the surface where the interface position is unknown. To document these aspects, micropillars were machined within a ferrite grain near the interface as well as in the interior of the ferrite grain. Specifically, one ferrite grain with a surface normal of [5 2 6] was selected and three micropillars were milled, one in the vicinity of the center of the grain and two others located diametrically opposite each other in the vicinity of the ferrite/martensite interface. The milled micropillar in the center of the grain had an orientation close to that for ferrite micropillar 2 in Fig. 4a. Pillar diameters were close to 1 μm so that they could be machined within a single ferrite grain. The heights of these micropillars were accordingly reduced to maintain the aspect ratio used previously for the other pillars (aspect ratio ⩾2). The compression stress–strain curves for the three micropillars are shown in Fig. 6a. It can be seen that the micropillar excised from the interior of the ferrite grain is weaker than the two ferrite micropillars milled close to the ferrite/martensite interface, a finding consistent with the nanoindentation data. The SEM images of the three

Please cite this article in press as: Ghassemi-Armaki H et al. Deformation response of ferrite and martensite in a dual-phase steel. Acta Mater (2013), http://dx.doi.org/10.1016/j.actamat.2013.10.001

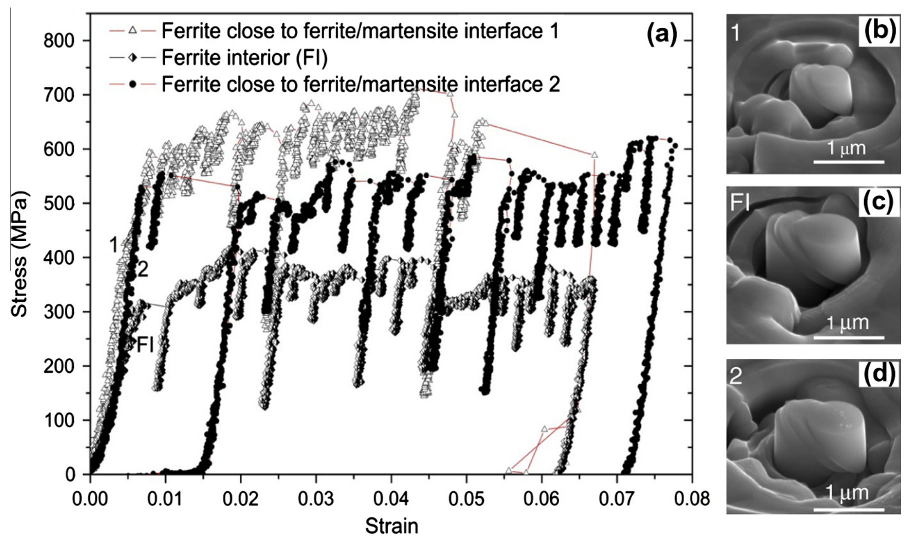

Fig. 6. (a) Compression engineering stress–engineering strain curves for three micropillars within a ferrite grain, with one located in the interior and two close to the ferrite/martensite interface in the same grain (the loading axis is [5 2 6]). (b–d) SEM images of the deformed pillar confirming that the deformation response is similar in all three cases.

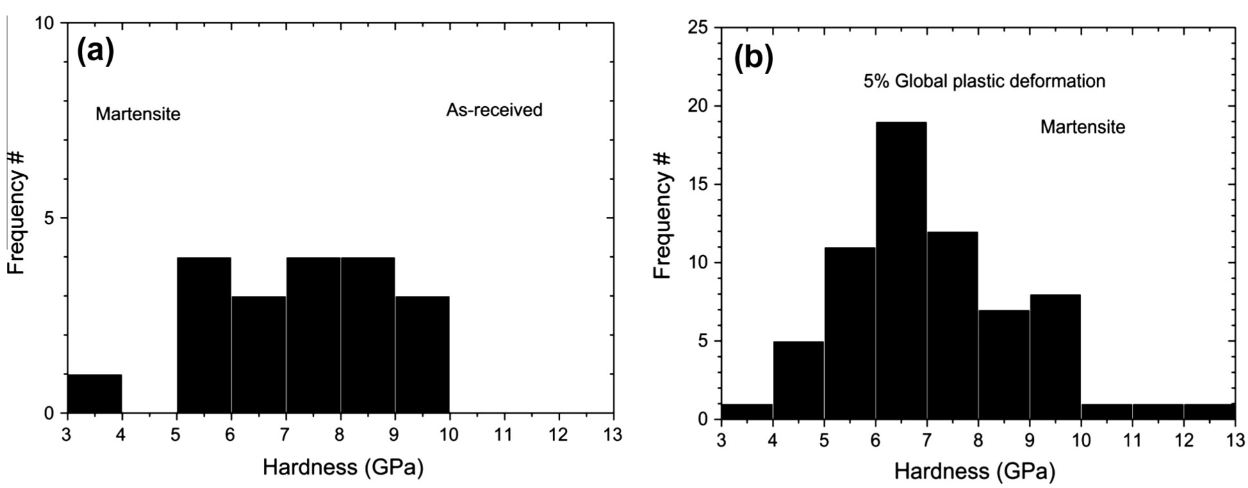

Fig. 7. Nanohardness distribution for martensite in the dual-phase steel in (a) the as-rolled condition and (b) after 5% plastic deformation in tension of the dual-phase steel.

deformed micropillars are shown in Fig. 6b–d and it is noted that the deformation response by the way of slip offset pattern (single slip on parallel planes) is reproducible in the three micropillars extracted from the single ferrite grain.

3.2.2. Martensite

The martensite phase in the dual-phase steel was similarly characterized. Initial studies on the nanoindentation of martensite confirmed a broad distribution in hardness, ranging from 3 to 10 GPa in the as-received dual-phase steel specimen (Fig. 7a) and from 3 to 13 GPa in the steel that had been pre-strained by 5% (Fig. 7b). The martensite in this steel has a hierarchical microstructure, with length scales ranging from ~10 μm (prior austenite grain size) to ~50 nm (individual lath widths). Consequently, nanoindentations that are of the order of 50–100 nm in contact depth and with a volume of influence extending a few hundred nanometers radially sample some of these microstructural length scales at each location but not others, and result in a spread of hardness values. In this study, we were not able to correlate nanoindentation hardness values to detailed substructures of martensite (laths, blocks or packets), making it difficult to delineate the effects of global deformation of the steel on the martensite phase (for example, compare Fig. 7a and b). As an alternative, micropillars of martensite were milled and deformed in compression to determine if more meaningful information could be obtained.

On average, the martensite islands were smaller than the ferrite grains, and this required reducing the martensite micropillar diameter to around 1.5 μm; the pillar height was typically ⩾3 μm, providing an aspect ratio ⩾2. A pillar of these dimensions will include several laths, and

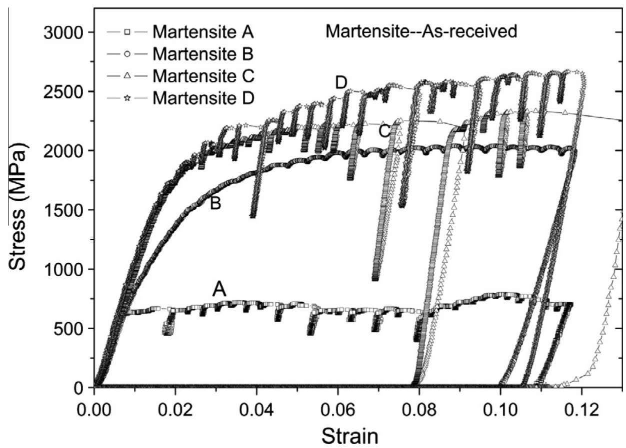

Fig. 8. Varied compression response (engineering stress–engineering strain curves) of four micropillars (A–D) excised from martensite. Pillars C and D are similar, whereas A and B are different. See text for further explanation.

possibly a few blocks and packet boundaries, in its volume. The compression stress–strain curves for four such martensite micropillars, A, B, C and D, are presented in Fig. 8. The curve for specimen A is markedly lower in yielding onset and plastic flow response relative to specimens C and D; furthermore, specimen B also exhibits a lower stress for yield onset compared to C and D, and is similar to or slightly higher than that for A; the subsequent flow response of specimen B could be considered comparable to that for C and D within the margin of uncertainty. Curves C and D overlap in the early stages but show some differences beyond about 2% plastic strain. To understand the origin of this scatter in stress–strain response, TEM samples from the deformed micropillars A, B and C were extracted by the FIB lift-out technique and examined in the bright-field mode and using selected area diffraction; these results are presented in Figs. 9–11. A reference SEM image of the deformed martensite micropillar A with a height of around 3 μm is shown in Fig. 9a; a low-magnification TEM image of a vertical section of the pillar is shown in Fig. 9b and a selected area diffraction pattern obtained from a location in the lower half of Fig. 9b is shown in Fig. 9c. The low-magnification TEM image in Fig. 9b corresponds to about 2.5 μm in the vertical direction which is about the overall height of the deformed pillar. About 0.8 μm from the top surface in Fig. 9b, a boundary is observed to traverse the entire section of the pillar and the material above it is martensite whereas the diffraction pattern in Fig. 9c confirms the entire microstructure below it to be ferrite, with fine Fe-carbides dispersed within it. Evidently, the martensite observed on the specimen surface only extends 0.8 μm below the surface, the rest of the pillar being ferrite. The compression response observed for specimen A in Fig. 8, illustrating a low stress for the onset of yielding and the absence of any work hardening, must correlate to the subsurface ferrite deformation.

A similar analysis of pillar B was undertaken and the observations are captured in Fig. 10a–d. A reference SEM image of the deformed micropillar B with a height of ∼3 μm is shown in Fig. 10a and a low-magnification TEM image of the vertical cross-section of the micropillar is provided in Fig. 10b. The electron-transparent area of the TEM micrograph covers approximately the height of the deformed micropillar B. In the TEM image, for a depth of about 1.4 μm, the microstructure is composed of what appears to be a fine subgrain structure, suggesting a breakdown of the lath microstructure; the diffraction pattern of this region shown in Fig. 10c confirms a polycrystalline structure (a discontinuous ring pattern). However, selected area diffraction from the region marked F in Fig. 10b (shown in Fig. 10d) and corresponding to the bottom of the micropillar confirms the presence of single crystalline ferrite. Thus a small amount of ferrite is included in the bottom of the micropillar B and affects the compression response in Fig. 8, though the effect is not as substantial as in micropillar A.

The deformed martensite micropillar C is shown in Fig. 11(a) and the corresponding TEM image of the vertical section is shown in Fig. 11b. The SEM image once again confirms the micropillar height to be in the vicinity of 3 μm, while the vertical section in the TEM bright field image spans ∼3.6 μm, suggesting that all of the pillar

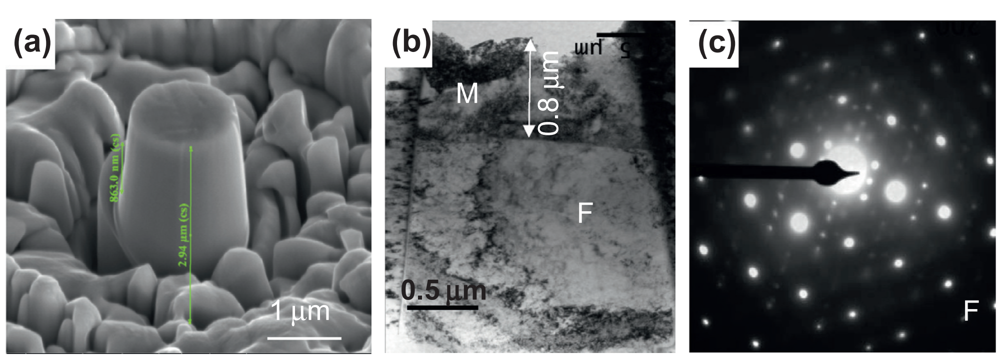

Fig. 9. (a) SEM image, (b) bright-field TEM image of vertical section obtained by FIB lift-off and (c) selected area diffraction image of the deformed micropillar A (in Fig. 8). The diffraction pattern confirms that there is a ferrite region (F) under the top layer of martensite that extends only about 0.8 μm below the surface.

Please cite this article in press as: Ghassemi-Armaki H et al. Deformation response of ferrite and martensite in a dual-phase steel. Acta Mater (2013), http://dx.doi.org/10.1016/j.actamat.2013.10.001

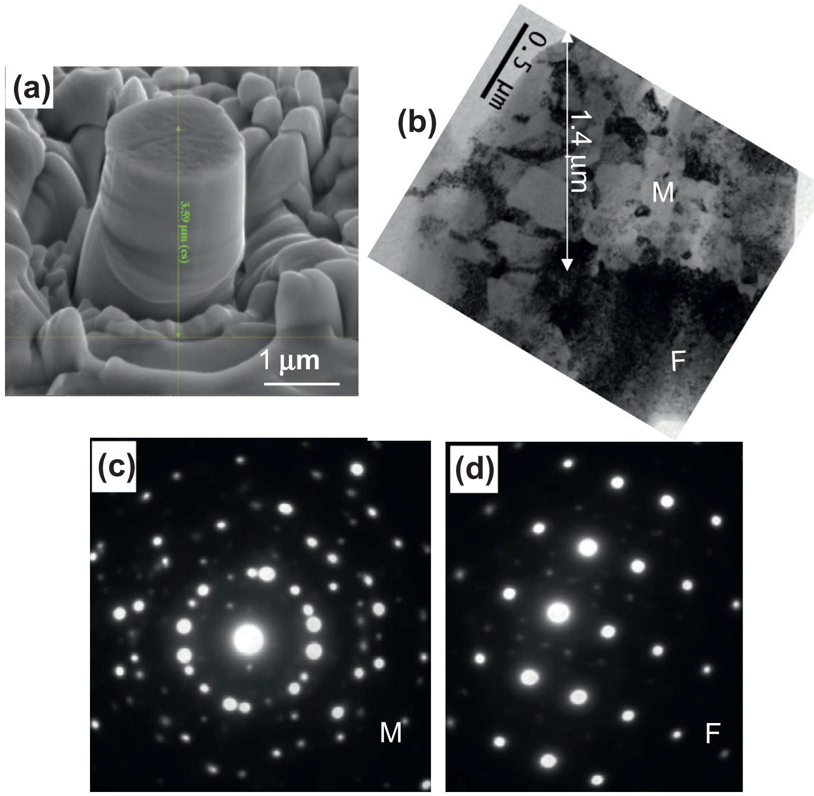

Fig. 10. (a) SEM image, (b) bright-field TEM image of vertical section obtained by FIB lift-off and (c and d) selected area diffraction images of the deformed micropillar B (in Fig. 8). Diffraction pattern (c) confirms that martensite (M) extends through most of the pillar height but (d) shows the presence of ferrite (F) in the lowest portion of the pillar.

microstructure, if not more, is captured in the image. The TEM sample is divided into four parts by the white double end-arrowed markers, and three of the parts are labeled (c), (d) and (e). Higher-magnification bright-field TEM images from each of these three parts are presented in Fig. 11c, d and e, respectively. As seen, the three images show that a martensite lath structure prevails throughout the vertical section. Therefore, we conclude that the compression stress–strain curves C and D in Fig. 8 are the appropriate curves depicting the mechanical response of the martensite phase in the dual-phase steel. As seen in the curves corresponding to micropillars C and D in Fig. 8, the yielding onset for the martensite phase is around 1 GPa.

3.3. Micromechanical response of pre-strained samples

The deformation behavior of the ferrite and martensite phases was tracked as a function of the strain imparted to the dual-phase steel in a tensile test. This was done to investigate how the individual phases accommodated the overall plastic deformation. We report the nanoindentation and micropillar compression responses of ferrite and martensite in tensile specimens of the dual-phase steel that had been strained to 0.5% and 7% strain. The 0.5% strain (corresponding to 800 MPa stress – Fig. 1f) is when the high work hardening rate following initial yielding at ~350 MPa gives way to a reduced work hardening rate, which appears as an "apparent second yielding event" in the uniaxial tension curve of the dual-phase steel (Fig. 1b), and the 7% strain corresponds to an extended excursion into the plastic regime prior to necking. At least three micropillars were evaluated for each strain for each phase, but only a representative curve is presented in each instance.

3.3.1. Ferrite

An SEM image of the dual-phase steel after 7% tensile strain is shown in Fig. 12a, with six nanoindentation impressions in the field of view: three on the left, marked 1, 2 and 3, and three on the right, marked 4, 5 and X. The middle indentation in the right side, marked X, was located partially on the ferrite/martensite interface and therefore ignored. Indentations 1 and 2 are inside the ferrite away from any interface, while 3, 4 and 5 are in the vicinity of the ferrite/martensite interface. The force–displacement curves resulting from the five nanoindentation tests (1–5 in Fig. 12a) are shown in Fig. 12b. The contact depth of indentations 1 and 2 are similar, with a hardness of 4.1 GPa, whereas the contact depths of indentations 3, 4 and 5 are larger, with hardness values in the range of 1.2–3.1 GPa. These results imply that in the 7% pre-deformed material the region close to the ferrite/martensite interface is softer than the interior ferrite, and is the converse response to that observed in the as-received material

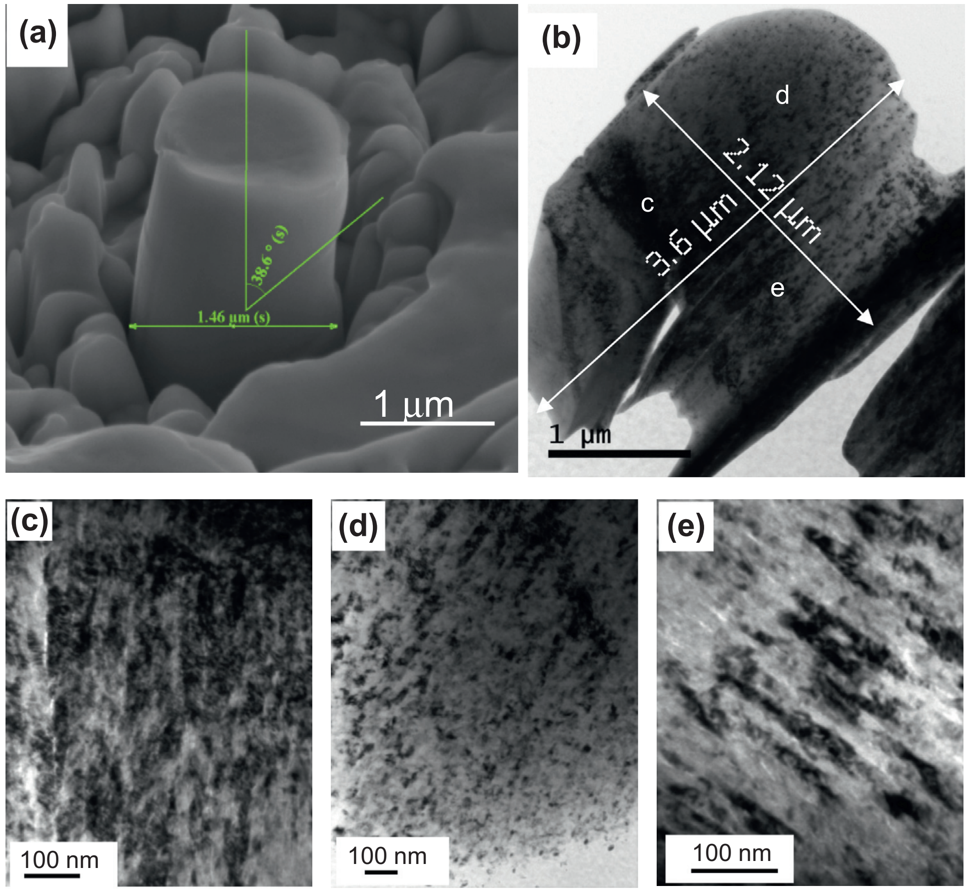

Fig. 11. Microstructural observations of deformed micropillar C (in Fig. 8) prepared by FIB milling: (a) SEM image and (b) low-magnification bright-field TEM image of the entire vertical section of the milled pillar. The image is divided into four sections, three of which are labeled c, d and e. (c–e) Higher-magnification bright-field TEM images of the locations marked c, d and e in (b) confirm the presence of the lath martensite morphology.

(compare Fig. 12b with Fig. 2b). Several indentations were made on the polished surface of the 7% tensile deformed specimen and the data were binned as previously described. The hardness distribution is presented as cumulative percent undersize plots in Fig. 12c–e. After 7% tensile strain in the dual-phase steel specimen, the ferrite in the grain interior is harder than ferrite near the ferrite/martensite interface (Fig. 12c). As mentioned above, this is different from that observed in the as-received specimen, where the ferrite in the vicinity of the ferrite/martensite interface was harder than the ferrite in the interior (Fig. 2c). This change appears to have been accomplished by the ferrite in the interior becoming harder (Fig. 12d) and the ferrite near the interface becoming softer (Fig. 12e).

The compression stress–strain data for the ferrite micropillars milled from tensile specimens that had been stretched to 0.5% and 7% plastic strain are provided in Fig. 13a. The yielding onset for the ferrite micropillar excised from the 0.5% pre-strained dual-phase steel sample was around 400 MPa (Table 1), and is almost the same as that for ferrite in the as-received condition. Following yielding, the specimen exhibits some hardening and attains a maximum flow stress in the vicinity of ~500 MPa (Fig. 13a). The compression stress–strain curve corresponding to the micropillar specimen extracted from the dual-phase steel tensile specimen that had experienced 7% plastic strain shows that yielding onset is around 450–500 MPa (Table 1) and there is a subsequent maximum in flow stress at around 650 MPa (Fig. 13a), suggesting work hardening of the ferrite during plastic flow of the dual-phase steel.

3.3.2. Martensite

The micropillar compression response for the martensite phase is shown in Fig. 13b; these micropillars were extracted from deformed dual-phase tensile specimens that had seen strains of 0.5% and 7%. Multiple micropillar specimens for each condition were tested to ensure reproducibility, and the response shown in Fig. 13b is representative of each condition. The onset of yielding was determined as before by plotting $d\sigma/d\varepsilon$ vs. σ, and these data for the as-received martensite micropillar C in Fig. 8 and for those in Fig. 13b are compared in Fig. 14. The yielding onset after 0.5% prior plastic tensile strain is ~1250 MPa, as compared to ~1 GPa in the as-received condition. Thus, even in the early stage of plastic deformation of the dual-phase steel, the martensite exhibits substantial hardening. The stress–strain curves for the

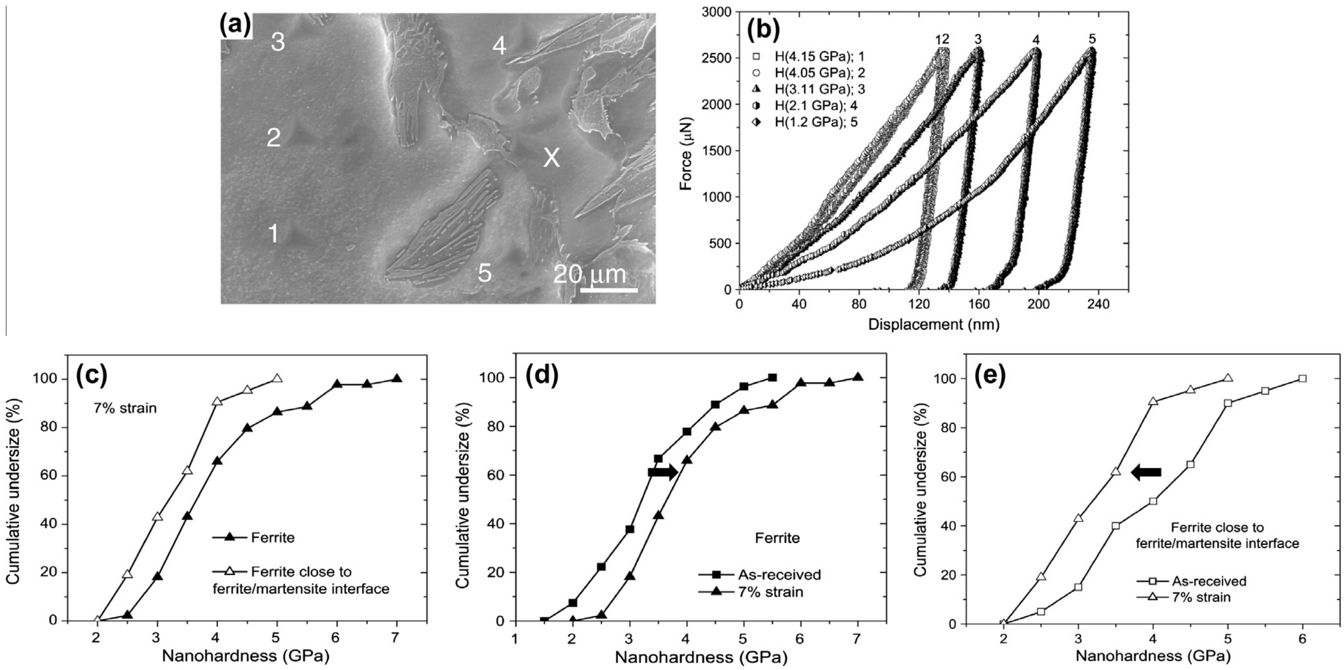

Fig. 12. (a) SEM image of the dual-phase steel after it had been subjected to 7% strain in uniaxial tension. The image shows six nanoindentation impressions that are labeled 1–5 and X. 1 and 2 are in the interior of a ferrite grain, whereas 3–5 are located in the ferrite close to the ferrite/martensite interface; X straddles the interface. (b) Force–displacement curves corresponding to nanoindentations 1–5. (c) Comparison of the nanohardness distribution (cumulative undersize plot) for ferrite in the interior and ferrite close to the ferrite/martensite interface following this 7% tensile strain of the dual-phase steel. (d and e) The consequence of the 7% global plastic strain on the hardness shift in the "interior" ferrite and on the ferrite close to the ferrite/martensite interface compared to the as-received condition.

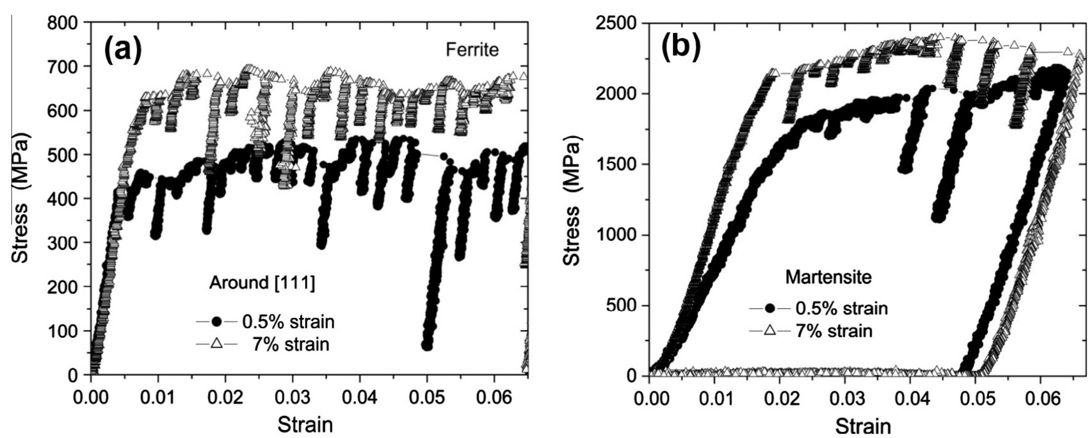

Fig. 13. Compression engineering stress–engineering strain curves for micropillars of (a) ferrite and (b) martensite obtained from tensile specimens of the dual-phase steel that had been deformed to 0.5% and 7% strain.

martensite micropillars milled from the tensile specimens that had experienced 7% strain showed yielding onset around ~1700 MPa; this is followed by further hardening up to ~2500 MPa (Fig. 13b). These results suggest that the hardening of martensite continues until at least the ultimate tensile strength (UTS) of the dual-phase steel.

4. Discussion

We have used micropillar compression tests to obtain the stress–strain response of the individual phases (ferrite and martensite) in a dual-phase steel in the as-received condition, as well as after subjecting the dual-phase steel to known levels of tensile strain; we have used the information to explain some aspects of the tensile stress–strain response of the dual-phase steel. In addition, we have used the observations from these micropillar tests to validate the results obtained from nanoindentation of the individual phases. The diameters of the ferrite and martensite micropillars were selected such that the size could be accommodated within the scale of the microstructure in the dual-phase steel. The ferrite in the as-received dual-phase sheet steel has a high dislocation density and includes finely spaced (~10–20 nm) carbide particles (Fig. 1b and c).

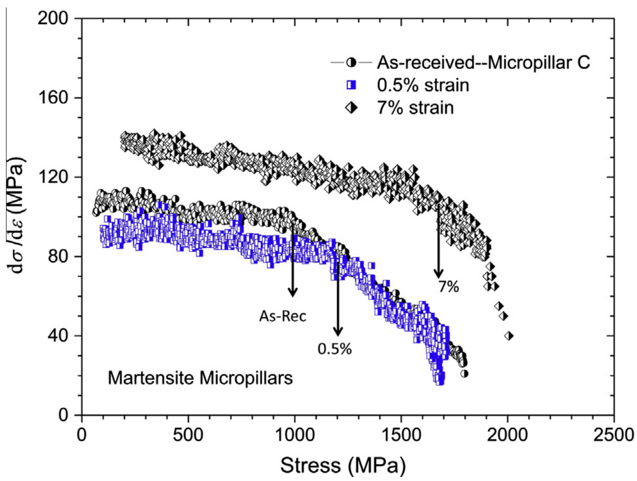

Fig. 14. Hardening rate vs. stress for micropillar compression of martensite specimen C in Fig. 9 and for the martensite micropillars extracted from tensile specimens of the dual-phase steel that had been deformed to 0.5% and 7% strain in Fig. 13b.

Recent work on micropillar deformation of oxide-dispersion-strengthened Ni-based superalloys has confirmed that internal obstacle spacing dominates the deformation behavior, with size effects being secondary [56]. The observation of onset of yielding in the ferrite pillars in the vicinity of 350–450 MPa and aligning with the onset of initial yielding in the dual-phase steel indirectly supports this argument.

Low-carbon lath martensite exhibits a hierarchical microstructure composed of laths, blocks, packets and prior austenite grain boundaries. The laths typically range in width from 30 to 300 nm, and several of them are included in micropillars that have a diameter of 1–2 μm and an aspect ratio of 2–4. In fully martensitic steels, it is reported that martensite blocks tend to be in the 1–10 μm range, while packet sizes depend almost linearly on the prior austenite grain size and can range from 5 μm to as high as 100 μm or more [57]. In the dual-phase steel examined in this study, the individual martensite islands are $\leqslant$10 μm in size (see Fig. 1a, for example) and limit the dimensions of the microstructural features such as blocks and packets to within those dimensions (Fig. 1d). Thus, the martensite micropillars examined in this investigation are thought to include block boundaries and even packet boundaries, both of which are known to be high-angle boundaries [57]. Therefore, the compression stress–strain response of the martensite micropillars is thought to be representative of a polycrystalline material and of the deformation behavior of martensite structure in the dual-phase steel.

In this context, we draw attention to the strength of the micropillar technique in determining the mechanical response of individual phases in a multiphase alloy in that the pillars are free-standing and devoid of constraints of adjacent phases while including all the microstructural and chemistry aspects present in the multiphase alloy, such as dislocation content, precipitates, consequences of prior heat treatment on solute distribution (or partitioning) and of phase transformations on microstructure of the individual phases that cannot be all captured in an “artificially produced” single phase alloy intended to represent a phase in the multiphase alloy. Furthermore, coupling the mechanical testing of micropillars with EBSD enables orientation-dependent responses (yield and hardening behavior) in variously processed/deformed conditions, which serve as useful and important input for computations, to be readily obtained. Nevertheless, there are some shortcomings as well. For example, tension/compression asymmetry and non-Schmid effects present in certain crystal structures are not accounted for and specifically, in this study, the deformation of bcc ferrite micropillars in compression is being used to interpret the tensile response of the dual-phase steel.

Nanoindentation and micropillar compression tests confirmed that plastic deformation of ferrite is not spatially homogeneous in that the strength of the ferrite adjacent to the ferrite/martensite interface is higher than that in the interior of the grain in the as-received condition (Fig. 2c). This strength inhomogeneity has been previously reported by others using nanoindentation [5,19,24] and attributed to the presence of GNDs resulting from the austenite-to-martensite transformation in the vicinity of the interface. Through in-situ tensile tests using synchrotron X-ray diffraction, Yu et al. [58] showed that, in a dual-phase steel of similar tensile strength level, strain distribution within a ferrite grain is inhomogeneous, and inferred that stress distribution in the ferrite grain must also be inhomogeneous.

The GNDs are thought to be mobile, whereas the dislocations in the interior of the ferrite are thought to be less so due to carbon segregation and/or carbide precipitation. During subsequent tensile deformation, these mobile unpinned dislocations in the vicinity of the interface can interact with each other and annihilate, or glide to the interior of the ferrite and interact with the immobile dislocations and influence the early stage strain hardening response of the steel. Thus, when the ferrite phase in the previously deformed dual-phase steel tensile specimens is investigated, the interior hardens relative to the as-received condition while the ferrite adjacent to the ferrite/martensite interface softens.

The first evidence for the onset of yielding in uniaxial tension of the dual-phase steel in Fig. 1f occurs at ~350 MPa and is attributed to the plastic deformation of ferrite. In this context, a range of yield stress (250–450 MPa) has been reported for polycrystalline ferrite as determined by Berkovich [25] and spherical [26] indenters, as well as for single-phase ferrite in a uniaxial tensile test [5]. The micropillar compression stress–strain curve for martensite exhibits a high initial hardening rate and reaches a maximum (plateau) strength of ~2.4 GPa (e.g. specimen C in Figs. 9 and 14). As seen in Fig. 14, the hardening rate of the martensite micropillar extracted from the as-received sheet changes at around 1 GPa, which is taken to represent the yielding onset of martensite. In a previous study [59] of the flow behavior of the martensite phase in a dual-phase steel with 0.3 wt.% carbon and roughly equal volume fractions of ferrite and martensite ($V_f \sim 50\%$), using neutron diffraction it was shown that martensite remains elastic until necking occurs in the steel and it was claimed that the martensite yielded at around 2.2 GPa, which is significantly higher than that observed in the present study. However, the martensite in Ref. [59] had a much higher carbon content (∼0.6% C) than does the martensite in the dual-phase steel examined here (∼0.3% C), and it is well known that carbon content has a significant influence on the strength of martensite.

Although the initial deviation from linearity in the vicinity of 350 MPa on the tensile stress–strain curve of the dual-phase steel can be associated with the onset of plastic flow in ferrite, the onset of plastic deformation of martensite is not obvious on the tensile stress–strain curve of the dual-phase steel, as has been previously noted [14,15,17,18]. Since the martensite pillar data in Fig. 14 confirms that the martensite yields at ∼1 GPa, we note that martensite plastic deformation in the dual-phase steel commences somewhere between 350 MPa and 1 GPa. The volume fractions of ferrite and martensite are approximately 0.6 and 0.4 for this steel, respectively; beyond 350 MPa, where ferrite yields in the dual-phase steel, recognizing that ferrite's ability to work harden is not appreciable, it is expected that stress and strain partitioning between the two constituent phases changes and martensite supports most of the stress. Thus, as shown in Fig. 1f, martensite plastic flow is thought to commence well below 1 GPa, with martensite work hardening beyond that stress level. The exact manner in which stress and strain partition between the two phases along the global stress–strain curve in Fig. 1f is not known and requires microstructure-calibrated crystal plasticity calculations. This is the subject of a subsequent paper targeted at predicting the stress–strain response of such dual-phase steels.

Thus plastic deformation and hardening of martensite occur fairly early in the stress–strain response of a dual-phase steel (∼0.5% plastic strain) and the subsequent loss in hardening capacity of the steel is associated with the loss in the hardening capacity of the martensite. These observations are also supported by the increased yielding onset stress for martensite micropillar compression specimens excised from previously deformed dual-phase tensile specimens that had been interrupted at 0.5% plastic strain and 7% plastic strain, the latter strain being less than the strain at UTS. The fact that the yielding onset stress in these pillars is higher than in the as-received martensite implies that plastic deformation had commenced in martensite when the dual-phase steel had experienced as little as 0.5% plastic strain. In other words, strain partitioning occurs early in global deformation, and both ferrite and martensite phases participate in accommodating the global strain.

In summary, we conducted uniaxial micromechanical experiments on the individual phases, ferrite and martensite, in a dual-phase sheet steel in the as-received and prestrained conditions. These findings provide for a mechanistic interpretation of the global stress–strain curve in the dual-phase steel. The behavior of the individual phases is used as input into microstructurally informed crystal plasticity-based computations that take into account latent hardening, non-Schmid effects and the hierarchical microstructural details of low-carbon lath martensite, and enable extraction of stress and strain partitioning in the phases with progress in global deformation of the steel. This work is in progress and will be reported subsequently.

5. Conclusions

Nanoindentation and micropillar compression tests of ferrite and martensite phases in a continuously annealed dual-phase sheet steel were performed in the as-received condition and after prior deformation. The primary findings are:

1. The hardness and strength of ferrite within individual ferrite grains are not spatially homogeneous in the as-received condition; the ferrite in the vicinity of the ferrite/martesite interface is harder and stronger than the ferrite in the grain interior.
2. In subsequent tensile deformation of the dual-phase steel, the ferrite in the interior work hardens while the ferrite near the ferrite/martensite interface softens; the inhomogeneous response persists at least up to 7% global plastic strain of the dual-phase steel.
3. The onset of yielding in ferrite in compression occurs at around 395 MPa and the subsequent hardening response is orientation dependent, being highest for the [0 0 1] loading axis.
4. Micropillar compression experiments confirm that martensite yields at ∼1 GPa and hardens rapidly until ∼1.5 GPa, then continues to harden more gradually to ∼2.3–2.5 GPa.
5. The initial yielding of the dual-phase steel correlates well with the onset of plastic deformation of ferrite. Importantly, however, it is shown that onset of plastic flow and hardening of martensite commence well before the ultimate tensile strength is reached in the dual-phase steel.
6. These microscale experiments provide important information and insights into the deformation characteristics of the individual phases that can then serve as valuable input into microstructurally informed computations aimed at predicting the flow behavior of these multiphase alloys in various stress states.

Please cite this article in press as: Ghassemi-Armaki H et al. Deformation response of ferrite and martensite in a dual-phase steel. Acta Mater (2013), http://dx.doi.org/10.1016/j.actamat.2013.10.001

Acknowledgements

Brown University acknowledges support from ArcelorMittal Global R&D East Chicago. Mechanical testing of the micropillars and post-deformation microstructural characterization were performed at Brown University using the Experimental Shared Facilities that is supported by the NSF-MRSEC on Micro- and Nano-Mechanics of Structural and Electronic Materials (NSF Grant DMR-0520651) at Brown University. J.R.G. and R.M. acknowledge the infrastructure and support of the Kavli Nanoscience Institute, the Alexander von Humboldt Foundation for the financial support to R.M. (and R.M.'s host, G.M. Pharr) and J.R.G.'s ONR Grant (N000140910883).

References

[1] Furukawa T, Tanino M, Morikawa H. Endo M Trans ISIJ 1984;24:113.
[2] Davies RG. Metall Trans A 1978;9A:41.
[3] Kim NJ, Thomas G. Metall Trans A 1981;12A:483.
[4] Nakagawa AH, Thomas G. Metall Trans A 1985;16A:831.
[5] Kadkhodapour J, Schmauder S, Raabe D, Ziaei-Rad S, Weber U, Calcagnotto M. Acta Mater 2011;59:4387.
[6] Erdogan M. J Mater Sci 2002;37:3623.
[7] Ciao XL, Feng J, Owen WS. Metall Trans A 1985;16A:1405.
[8] Bag A, Ray KK, Dwarakadasa ES. Metall Mater Trans A 1999;30:1193–202.
[9] Tomita Y. J Mater Sci 1990;25:5179–84.
[10] Byun TS, Kim IS. J Mater Sci 1993;28:2923.
[11] Tomota Y. Mater Sci Technol 1987;3:415–21.
[12] Chen HC, Cheng GH. J Mater Res 1989;24:1991.
[13] Balliger NK, Gladman T. Met Sci 1981;15:95.
[14] Marder AR. Metall Trans A 1982;13:85.
[15] Kang JD, Ososkov Y, Embury JD, Wilkinson DS. Scr Mater 2007;56:999.
[16] Kim EY, Yang HS, Han SH, Kwak JH, Choi SH. Met Mater Inter 2012;18:573.
[17] Calcagnotto M, Adachi Y, Ponge D, Raabe D. Acta Mater 2011;59:658.
[18] Jiang ZH, Guan ZZ, Lian JS. Mater Sci Eng A 1995;190:55.
[19] Sun X, Choi KS, Soulami A, Liu WN, Khaleel MA. Mater Sci Eng A 2009;526:140.
[20] Korzekwa DA, Matlock DK, Krauss G. Metall Trans A 1984;15:1221.
[21] Calcagnotto M, Ponge D, Demir E, Raabe D. Mater Sci Eng A 2010;527:2738.
[22] Sarosiek AM, Owen WS. Mater Sci Eng 1984;66:13.
[23] Oliver WC, Pharr GM. J Mater Res 2004;19:3.
[24] Kalidindi SR, Pathak S. Acta Mater 2008;56:3523.
[25] Delincé M, Jacques PJ, Pardoen T. Acta Mater 2006;54:3395.
[26] Choi BW, Seo DH, Yoo JY, Jang JI. J Mater Res 2009;24:816.
[27] Cao YP, Lu J. Acta Mater 2004;52:4023.
[28] Zhao M, Ogasawara N, Chiba N, Chen X. Acta Mater 2006;54:23.
[29] Greer JR, De Hosson JThM. Prog Mater Sci 2011;56:654.
[30] Kraft O, Gruber PA, Mönig R, Weygand D. Ann Rev Mater Res 2010;40:293.
[31] Dehm G. Prog Mater Sci 2009;54:664.
[32] Uchic MD, Shade PA, Dimiduk DM. Ann Rev Mater Res 2009;39:361.
[33] Greer JR, Nix WD. Phys Rev B 2006;73:245410.
[34] Uchic MD, Dimiduk DM, Florando JN, Nix WD. Science 2004;305:986.
[35] Cheng Y-T, Cheng C-M. J Mater Res 1999;14:3493.
[36] Bucaille JL, Stauss S, Felder E, Michler J. Acta Mater 2003;51:1663.
[37] Ohmura T, Tsuzaki K, Matsuoka S. Scr Mater 2001;45:889.
[38] Li J, Ohmura T, Tsuzaki K. Mater Trans 2005;46:1301.
[39] Nakajima M, Komazaki S, Kohno Y. Int J Press Vessels Piping 2009;86:563.
[40] Maaß R, Uchic MD. Acta Mater 2012;60:1027.
[41] Maaß R, Meza L, Gan B, Tin S, Greer JR. Small 2012;8:1869.
[42] Kim J-Y, Jang D, Greer JR. Acta Mater 2010;58:2355.
[43] Schneider AS, Kaufmann D, Clark BG, Frick CP, Gruber PA, Mönig R, et al. Phys Rev Lett 2009;103:105501.
[44] Brinckmann S, Kim J-Y, Greer JR. Phys Rev Lett 2008;100:155502.
[45] Weinberger CR, Cai W. Proc Natl Acad Sci 2008;105:14304.
[46] Greer JR, Weinberger CR, Cai W. Mater Sci Eng 2008;493A:21.
[47] Ghassemi-Armaki H, Chen P, Bhat S, Sadagopan S, Kumar S, Bower A. Acta Mater 2013;61:3640.
[48] Stewart JL, Jiang L, Williams JJ, Chawla N. Mater Sci Eng 2012;A534:220.
[49] Gianuzzi LA, Drown JL, Brown SR, Irwin RB, Stevie FA. Micros Res Technol 1998;41:285.
[50] Ito K, Vitek V. Philos Mag A 2001;81:1387.
[51] Brunner D, Diehl J. Mater Sci Eng 1993;164A:350.
[52] Caillard D. Acta Mater 2011;59:4974.
[53] Rosenberg JM, Piehler HR. Metall Trans 1971;2:257.
[54] Rauch GC, Leslie WC. Metall Trans 1972;3:373.
[55] Hirth JP, Cohen M. Metall Trans 1970;1:3.
[56] Girault B, Schneider AS, Frick CP, Arzt E. Adv Eng Matls 2010;12:385.
[57] Morito S, Yoshida H, Maki T, Huang X. Mater Sci Eng 2006;A438:237.
[58] Yu Z, Barabash R, Barabash O, Liu W, Feng Z. JOM 2013;65:21.
[59] Jacques PJ, Furnémont Q, Godet S, Pardoen T, Konlon KT, Delannay F. Philos Mag 2006;86:2371.

Please cite this article in press as: Ghassemi-Armaki H et al. Deformation response of ferrite and martensite in a dual-phase steel. Acta Mater (2013), http://dx.doi.org/10.1016/j.actamat.2013.10.001